







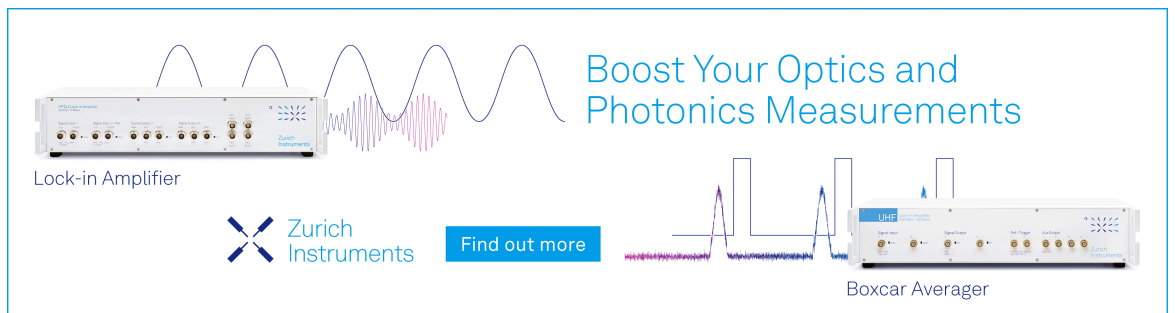
RESEARCH ARTICLE | APRIL 22 2024

Magnetization switching by electric field in ZnFe₂O₄/ZnO heterostructure

Suman Guchhait  ; H. Aireddy  ; Sudarshan Singh  ; Sayan Chakraborty  ; Niladri Sekhar Kander  ; A. K. Das  



J. Appl. Phys. 135, 164102 (2024)
<https://doi.org/10.1063/5.0204360>



Boost Your Optics and Photonics Measurements

Lock-in Amplifier

Zurich Instruments

Find out more

Boxcar Averager

Magnetization switching by electric field in ZnFe₂O₄/ZnO heterostructure

Cite as: J. Appl. Phys. **135**, 164102 (2024); doi: [10.1063/5.0204360](https://doi.org/10.1063/5.0204360)

Submitted: 21 February 2024 · Accepted: 8 April 2024 ·

Published Online: 22 April 2024



Suman Guchhait,¹ H. Aireddy,² Sudarshan Singh,¹ Sayan Chakraborty,³ Niladri Sekhar Kander,¹ and A. K. Das^{1,a)}

AFFILIATIONS

¹Department of Physics, IIT Kharagpur, Kharagpur, West Bengal 721302, India

²Department of Electronics and Communication Engineering, Alliance College of Engineering and Design, Bengaluru, Karnataka 562106, India

³School of Nano-Science and Technology, IIT Kharagpur, Kharagpur, West Bengal 721302, India

^{a)}Author to whom correspondence should be addressed: amal@phy.iitkgp.ernet.in

ABSTRACT

We have fabricated the ZnFe₂O₄/ZnO (ZFO/ZnO) heterostructure on a silicon substrate by pulsed laser deposition technique and studied the magnetization switching by the electric field in the ZFO/ZnO heterostructure using an indigenously developed optical cantilever beam magnetometer setup. The magnetization (M) vs electric field (E) curve reveals that the magnetization of the ZFO film has been switched by an electric field applied along the thickness of the ZnO film. The saturation magnetization is found to be 28.77 MA/m from the M–E curve. The emergence of electric field-driven magnetization switching in the ZFO/ZnO heterostructure is attributed to the strain-mediated magnetoelectric coupling between the electric polarization of the ZnO film and the magnetization of the ZFO film as evidenced by the butterfly-type hysteresis behavior of magnetization with the applied electric field. However, the realization of electric field-controlled magnetization switching in the ZFO/ZnO heterostructure is regarded as a potential aspect for the fabrication of energy-efficient spintronic devices such as magnetoelectric random access memory cells, highly sensitive magnetic field sensors, magneto-logic devices, and neuromorphic devices.

© 2024 Author(s). All article content, except where otherwise noted, is licensed under a Creative Commons Attribution (CC BY) license (<https://creativecommons.org/licenses/by/4.0/>). <https://doi.org/10.1063/5.0204360>

I. INTRODUCTION

The most promising development in next-generation electronic data processing technology is thought to be magnetoresistive random access memory (MRAM).^{1–4} High speed of operation, nonvolatility, unlimited endurance, high density, and low energy dissipation rate are only a few of its alluring benefits.^{5,6} The switching of magnetization is regarded to be the most essential requirement for writing a piece of information in a typical MRAM device, and for switching, one can adopt several strategies, for example, the use of a magnetic field,^{7,8} the implementation of spin-orbit-torque (SOT) mechanism,^{9–11} and spin transfer torque (STT) method.^{12–14} As we know that the magnetic field is non-localized by nature and, hence, the generation of a stray field during the magnetic field-driven magnetization switching is inevitable and may have an adverse effect on the environment.¹⁵ On the other hand, to switch the magnetization through the SOT or STT technique, we need to

produce a very high density of spin-polarized current ($\sim 10^7$ A/m²), which leads to an energy consumption of $(10^7\text{--}10^8)$ KT at room temperature.^{16–19} Such a huge energy loss inspires the scientific community to find better strategies for magnetization switching. In this case, the most advantageous method for creating the next generation of spintronic devices, which combine both ultralow energy consumption (\sim aJ) and extremely fast operation speeds, would be the switching of magnetization with the aid of a localized electric field, the so-called converse magnetoelectric effect (CME).^{20–24} To realize the electric field-assisted magnetization switching, one needs to incorporate a multiferroic (MF) material in an MRAM unit cell. Usually, MF materials are a class of materials where at least two ferroic orders (ferroelectric, ferromagnetic/anti-ferromagnetic/ferromagnetic, or ferroelastic) coexist, and subsequently, coupling happens between any two ferroic orders.^{25–27} An MF material is typically divided into two categories: (i) single-phase MF material in which the ferroelectric (FE) and ferromagnetic (FM) phases

26 May 2024 10:24:11

naturally coexist and magnetoelectric (ME) coupling occurs directly between the FE and FM phases,^{28,29} and (ii) double-phase MF material produced artificially by merging the FM and FE phases in the form of an FM/FE heterostructure system in which neither the FM nor the FE phase exhibits multiferroicity, but the system as a whole exhibit multiferroic property due to the ME coupling accomplished indirectly via induced strain.^{30,31} In the FM/FE heterostructure, the application of an electric field across the thickness of the bottom FE layer produces electrostrictive strain in the FE film due to the converse piezoelectric effect (CPE). Subsequently, this electrostrictive strain is mechanically transmitted to the upper FM layer and manipulates its magnetization through the converse magnetostriction effect.^{32–35} However, due to symmetry constraints, single-phase MF materials appear to be extremely rare.^{36,37} In this situation, it becomes obvious to use an FM/FE heterostructure system to realize the electric field-induced magnetization switching phenomena that would be used to create energy-efficient MRAM devices.^{38–41}

In this study, we have presented the electric field-induced magnetization switching in the ZFO/ZnO heterostructure at ambient temperature. This seems to have occurred as a result of strain-mediated ME coupling between the polarization of the ZnO film and the magnetization of the ZFO film. According to our findings, the converse piezoelectric effect (CPE) causes electrostrictive strain in the ZnO film when a DC electric field is applied across it. This electrostrictive strain is then mechanically transferred to the top ZFO film, where it affects the magnetization of the ZFO film by means of the converse magnetostriction effect. In this case, the heterostructure acts as a double-phase MF ME composite, where the magnetization of the ZFO film and polarization of the ZnO film are connected indirectly through strain. The implementation of the electric field control of magnetization in a ZFO/ZnO heterostructure is viewed as a promising aspect for the fabrication of energy-efficient spintronic devices.

II. EXPERIMENTAL DETAILS

A. Sample preparation

The ZFO/ZnO heterostructure has been prepared using the pulsed laser deposition (PLD) system, in which a focused KrF excimer laser source with a wavelength of 248 nm, an energy of 400 mJ, and a repetition rate of 10 Hz is used to ablate the ZFO and ZnO targets. First, we cleaned and masked both ends of the Si cantilever substrate with dimensions of length (l_s) = 25 mm, width (w_s) = 5 mm, and thickness (t_s) = 100 μm . The bare cantilever substrate is then placed inside a thermal evaporation chamber for the creation of the bottom Au electrode at a base pressure of 2×10^{-6} mbar. The ZnO layer is then formed on top of the Au/Si composite by the PLD technique at a base pressure of 1.2×10^{-5} mbar and a substrate temperature of 500 $^\circ\text{C}$. On top of the ZnO/Au/Si composite structure, an Au electrode is once more created using the thermal evaporation process under identical circumstances. Finally, utilizing the PLD system at base pressures of 2×10^{-5} mbar and substrate temperatures of 550 $^\circ\text{C}$, the ZFO film is deposited on top of the Au/ZnO/Au/Si heterostructure.

B. Structural measurement

For the structural characterization of the synthesized ZFO/ZnO heterostructure, we have conducted an x-ray diffraction

(XRD) study in θ - 2θ geometry with a Cu source of wavelength 1.54 \AA inside the angle from 20 $^\circ$ to 70 $^\circ$. The heterostructure is characterized through the field emission scanning electron microscope (FESEM) system to evaluate the thickness and layer-by-layer development of the films.

C. Electric field-controlled magnetization measurement

With the help of the optical CBM system, we have investigated the electric field-controlled magnetization of the ZFO/ZnO heterostructure at room temperature. In this study, electrostrictive stress is created at the interface of the ZnO film and Si substrate by applying DC bias (V) throughout the thickness (Z-direction) of the ZnO film. The top ZFO film receives the mechanical transmission of the induced electrostrictive stress, which rotates the magnetic moments of the ZFO film along its length (X-direction), and this leads to the bending of the ZFO/ZnO heterostructure. Now, when a small magnetic field (H_z) of 1.28 mT is applied along the thickness of the ZFO/ZnO heterostructure, it induces torque (T) along the width of the heterostructure [negative (–) Y-direction], which eventually causes the ZFO/ZnO heterostructure to deflect. So, here, the deflection (Δ) of the ZFO/ZnO heterostructure actually takes place due to the magnetization (M) of the ZFO film. In this study, the torque field is applied via a KEPCO 20-20 current source meter, while the electric field is applied by a KEYSIGHT B2961A voltage source meter. So, based on the deflection of the heterostructure, we computed the magnetization of the ZFO film by the following equation:

$$M = \frac{Y_s w_s t_s^3}{2V_f H_z} \left[\frac{\Delta}{3(b+a)(l_{\text{eff}} - b) + 2b(b+a) - a^2} \right]. \quad (1)$$

Here, Young's modulus, width, and thickness of the cantilever-Si substrate are represented by Y_s , w_s , and t_s , respectively, while the length, breadth, thickness, and volume of the ZFO film are denoted by $l_f (= b - a)$, w_f , t_f , and V_f , respectively. "a" and "b" are the distances of the near and far ends of the ZFO film from the clamped point ($x = 0$), while " l_{eff} " denotes the distance between the incident laser spot and the clamped position. Moreover, the torque field is represented by H_z . The numerical values of all these parameters are given in Table I.

Figure 1(a) schematically depicts the 3D perspective of the ZFO/ZnO heterostructure with the DC voltage applied across the thickness of the ZnO film. We have vectorially depicted the process of the electric field-induced magnetization measurement of the ZFO/ZnO heterostructure in Fig. 1(b), where T denotes the torque acting along the width [negative (–) Y-direction] of the ZFO film. Figure 1(c) depicts the heterostructure in its unstrained condition ($V = 0$ V and $H_z = 0$ mT). The strain state, where the heterostructure bends when the voltage is applied, is shown in Fig. 1(d).

III. RESULTS AND DISCUSSION

A. Structural characteristics

Figure 2(a) indicates the XRD profile of the ZFO/ZnO heterostructure. In the XRD spectra, the indexed peaks signify the formation of both the hexagonal wurtzite phase and cubic spinel phase

TABLE I. Numerical values of the variables necessary to compute the magnetization caused by an electric field in the ZFO/ZnO heterostructure.

Name of the variables	Numerical value
Young's modulus of the substrate (Y_s)	150 GPa
Width of the substrate (w_s)	5 mm
The thickness of the substrate (t_s)	100 μ m
Length of the film (l_f)	9 mm
Width of the film (w_f)	3 mm
The thickness of the film (t_f)	21.16 nm
Deflecting field (H_z)	1.28 mT
a	12 mm
b	21 mm
Effective length (l_{eff})	22 mm

associated with the ZnO film and ZFO film, respectively. The appearance of numerous peaks in the XRD profile demonstrates the polycrystalline nature of the fabricated ZFO/ZnO heterostructure. Consequently, the heterostructure is related to several domains. Figure 2(b) reveals the cross-sectional view of the ZFO/ZnO heterostructure captured by the MERLIN FESEM system at a magnification of 100.00 k. The figure depicts the sequential growth of the ZFO film and ZnO film on the Si substrate. Furthermore, the thickness of the ZFO and ZnO films has been examined using the FESEM image and found to be 21.16 and 28.31 nm, respectively.

B. Electric field-controlled magnetization characteristic

Figure 3(a) depicts the variation in the deflection (Δ) of the ZFO/ZnO heterostructure with the applied electric field (E). Now, in this study, we have computed the magnetization (M) of the ZFO film from the deflection of the ZFO/ZnO composite and illustrated its variation with the electric field in Fig. 3(b). According to Fig. 3(b), the magnetization vs electric field curve has appeared to be tensile in nature. Furthermore, we have found a butterfly-like parabolic hysteresis behavior of magnetization with the applied electric field. The sweep directions of the applied electric field are shown by the arrow marks in the corresponding figure. Now, one can infer from Fig. 3(b) that the magnetization of the ZFO film changes when an electric field is applied across the ZnO film in the ZFO/ZnO heterostructure. This is known as the converse magnetoelectric effect (CME), and it happens due to the ME coupling that occurs between the polarization (P) of the ZnO film and the magnetization of the ZFO film. Here, as we apply the electric field along the thickness of the ZnO film, electrostrictive strain is generated in the ZnO film because of the converse piezoelectric effect. Subsequently, the developed electrostrictive strain is mechanically transferred to the top ZFO film, where it modifies the domain magnetization of the ZFO film by means of the converse magnetostriction effect. Thus, in this study, a strain-mediated indirect ME coupling takes place between the polarization of the ZnO film and magnetization of the ZFO film, and as a result, the M-E curve has appeared in a butterfly shape. The saturation magnetization (M_{sat}) of the ZFO film has been obtained to be 28.77 MA/m from the

M-E curve. Now, the hysteresis nature of the M-E curve indicates that the ME coupling modifies the domain magnetization of the ZFO film in an irreversible way through the induced strain. Furthermore, the ZFO film is known to possess positive (+) in-plane magnetostriction.^{42,43} Therefore, the electrostrictive strain, which is mechanically conveyed to the ZFO film from the bottom ZnO layer through the ME coupling, causes the magnetic domains of the ZFO film to elongate, and as a consequence of this, we have found the tensile nature of the M-E curve as demonstrated in Fig. 3(b). Here, the presented M-E curve also dictates that the magnetization of the ZFO film varies as a square of the applied electric field, i.e., $M \sim E^2$, and hence, the M-E curve looks like a parabola. The switching of magnetization in the ZFO/ZnO heterostructure under the influence of an electric field has been explained through our presented M-E curve. Initially, the polarization vectors within each domain of the ZnO film are aligned at random when there is no electric field, i.e., $E = 0$. Now, due to the ME coupling, the orientation of the magnetic domain vectors in the ZFO film would also be random, and as a result, the net magnetization (M) is zero at $E = 0$. However, as the electric field is raised, initially the magnetization of the ZFO film falls and it continues until an electric field of $E_1 = 79.47$ MV/m is reached. At this field value, the polarization vectors associated with each domain of the ZnO film start to get aligned along the applied electric field. Now, as we increase the electric field beyond this, the polarization and, consequently, magnetization grow continuously. Finally, as we reach $E = E_{max}$ (211.94 MV/m), the polarization vectors corresponding to each domain of the ZnO film are perfectly aligned in the field direction (along the Z axis). Now, as a result of ME coupling, the resultant magnetization of the ZFO film gets aligned along its length, i.e., along the X axis. The respective alignments of polarization and magnetization in the ZFO/ZnO heterostructure at $E = E_{max}$ are shown schematically in Fig. 3(c). However, there is no additional domain reorientation in the heterostructure once the electric field is reduced. The polarization and, consequently, the magnetization decline gradually with a decrease in the electric field and, eventually, the magnetization becomes zero at $E = 0$. Now, as we reverse the electric field and attain a field $E_2 = -61.82$ MV/m, the polarization of the ZnO film starts to get aligned in the opposite direction. However, as we reach $E = -E_{max}$ (-211.94 MV/m), the polarization gets switched and directed along the -ve field direction (along the -Z axis). The direction of polarization is reversed at $E = -E_{max}$. Now, because of the ME coupling, the direction of magnetization of the ZFO film also gets flipped and it points toward the -X axis at $E = -E_{max}$. The orientations of polarization and magnetization vectors in the ZFO/ZnO heterostructure at $E = -E_{max}$ are illustrated schematically in Fig. 3(d). We have also indicated the direction of the electric field by the red arrow mark in Figs. 3(c) and 3(d). Therefore, we have observed the electric field-induced magnetization reversal in the ZFO/ZnO heterostructure, and this is due to the strain-mediated ME coupling between the polarization and magnetization vectors related to the corresponding heterostructure. So, the magnetization reversal in ZFO purely depends on the modulation of the polarization direction of the ZnO film. Here, the magnetic field (H_z) applied along the thickness of the ZFO/ZnO heterostructure induces a torque (T) along the width of the heterostructure [negative (-) Y-direction], which eventually causes the ZFO/ZnO

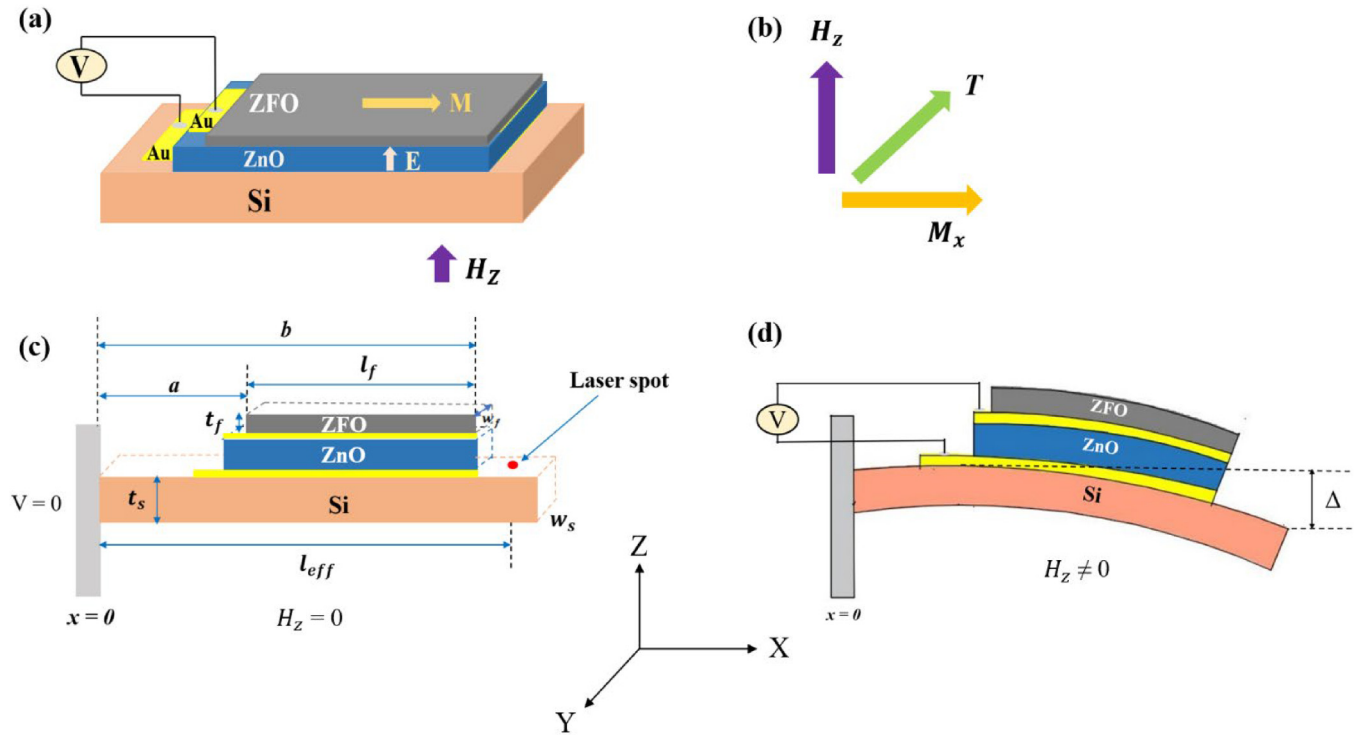


FIG. 1. (a) 3D block schematic of the ZFO/ZnO heterostructure in the presence of an electric and a deflecting field. (b) Vectorial representation of the method of electric field-controlled magnetization measurement in the ZFO/ZnO heterostructure. (c) Schematic representation of the ZFO/ZnO heterostructure in the absence of an electric field. (d) Schematic representation of the ZFO/ZnO heterostructure in the presence of an electric field.

26 May 2024 10:24:11

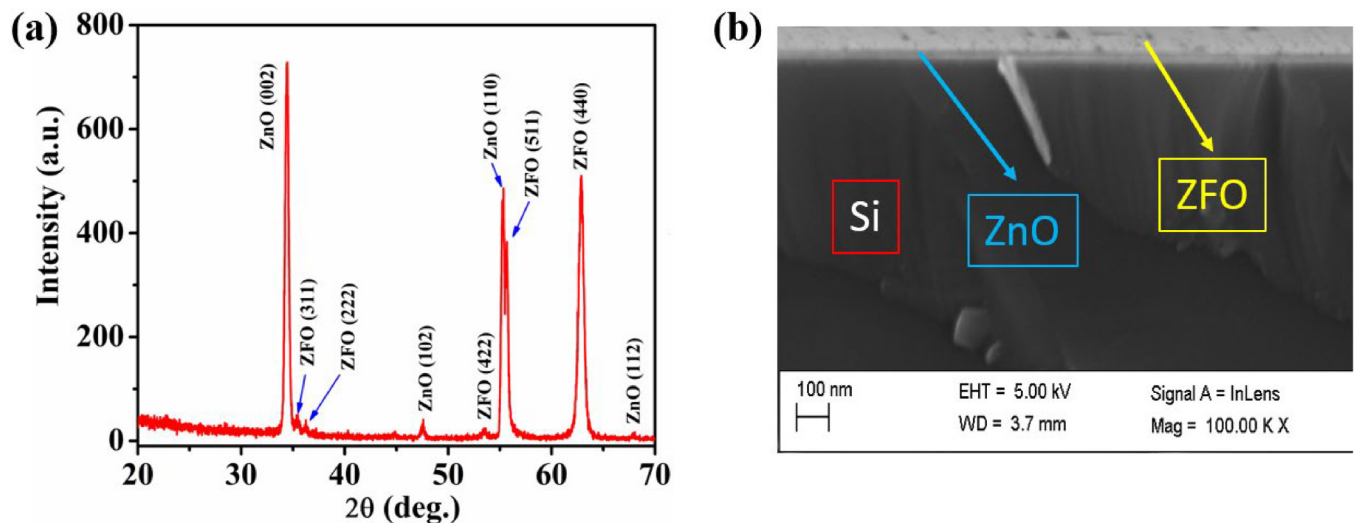
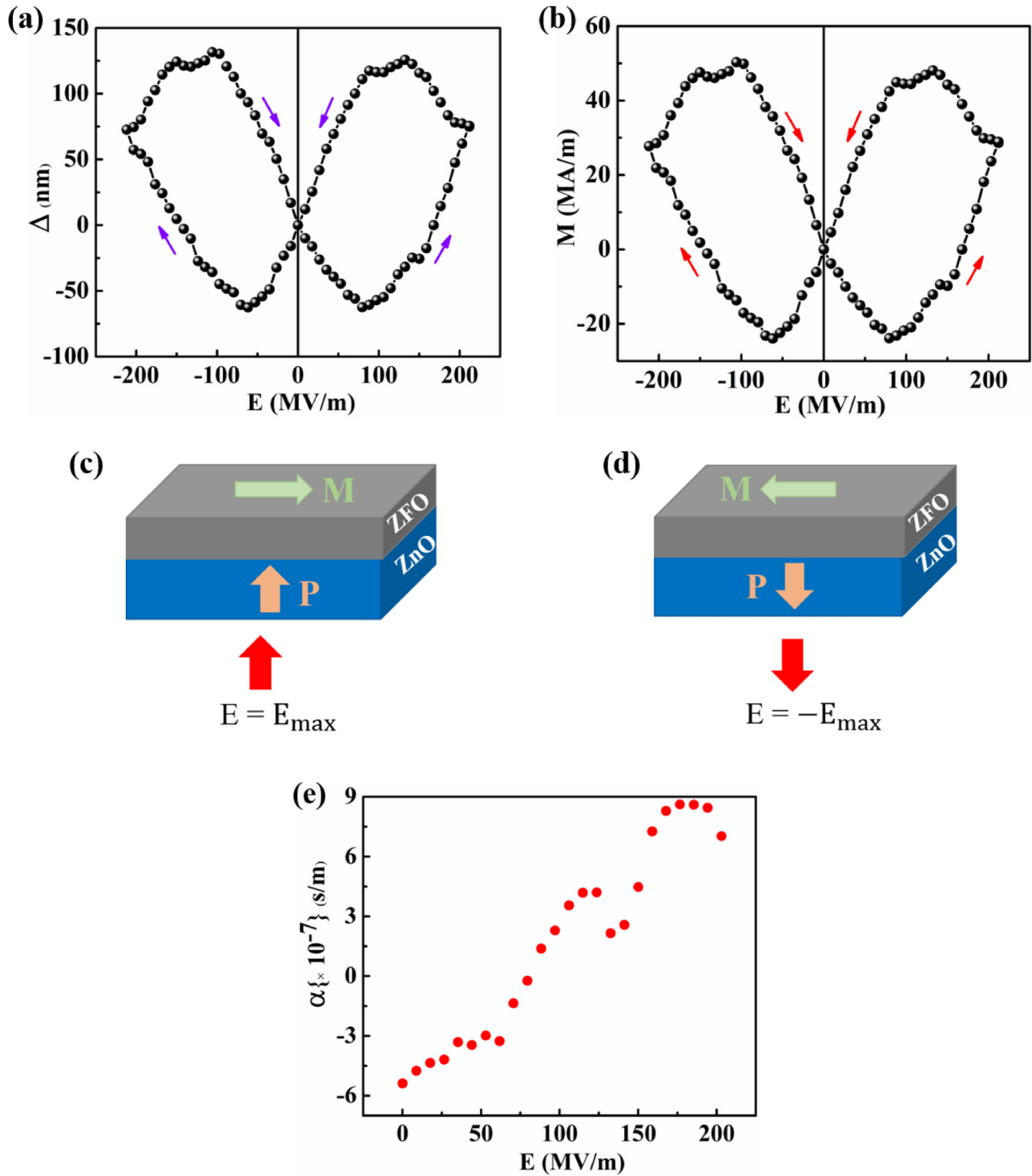


FIG. 2. (a) XRD profile of the ZFO/ZnO heterostructure obtained inside the angle from 20° to 70°. (b) Cross-sectional image of the ZFO/ZnO heterostructure captured through the MERLIN FESEM study.



26 May 2024 10:24:11

FIG. 3. (a) Deflection vs electric field curve for the ZFO/ZnO heterostructure. (b) Variation in electric field-induced magnetization with the applied electric field. (c) It shows how the polarization and magnetization vectors of the ZFO/ZnO heterostructure line up at an electric field of $E = E_{\max}$. (d) This reveals that the strain-mediated ME coupling causes the magnetization orientation of the ZFO film to be reversed in line with its initial alignment. (e) Change in the ME coupling coefficient with the applied electric field.

heterostructure to deflect. In addition, we have chosen the magnitude of H_z to be very small (1.28 mT) so that we can prevent the switching of magnetization along the direction of H_z . Therefore, H_z does not have any impact on the magnetization reversal in ZFO. The opposite trends of the M–E hysteresis curve [Fig. 3(b)] around the electric field of ~ 79 MV/m are mainly because of polarization switching in the ZnO film. The net polarization of the ZnO film directs toward the opposite direction with respect to the applied field up to this field value. In the ZFO/ZnO heterostructure, the polarization of the ZnO film is coupled with the magnetization of the ZFO film. Now, because of this coupling, the opposite sense of the polarization direction leads to the reduction in the magnetization of the ZFO film as the field is raised from zero to ~ 79 MV/m. However, as we reach the field value of ~ 79 MV/m, the polarization switching happens and the net polarization starts to get aligned along the applied field, which eventually increases the magnetization value of the ZFO film due to the coupling. A similar phenomenon occurs while reducing the electric field from its highest value. In this article, we have also presented a physical parameter known as the ME coupling coefficient (α), which actually determines the amount of ME coupling taking place between the polarization and the magnetization associated with the ZFO/ZnO heterostructure. The ME coupling coefficient is defined as the rate of change of magnetization in response to an applied electric field multiplied by the permeability of free space (μ_0). So, it is calculated as $\alpha = \mu_0 \frac{dM}{dE}$. Here, we have determined the values of α by considering the ascending cycle associated with the first quadrant of the M–E loop [Fig. 3(b)]. We have considered the (E, M) data from the M–E loop and calculated the dM/dE . Consequently, each dM/dE value is multiplied by μ_0 to get the separate α values. The variation in α with the applied electric field is illustrated in Fig. 3(e). In this investigation, the ZFO/ZnO heterostructure operates as a double-phase MF ME system in which the magnetization of the ZFO film is manipulated by the electric field. The appearance of the electric field tuning of magnetization in the ZFO/ZnO heterostructure is thought to be an extremely exciting aspect in order to create magnetoelectric random access memory (MERAM) elements, magneto-logic equipment, extremely delicate magnetic field sensors, and neuromorphic devices.^{44–46} In an MERAM element, the magnetization switching speed would be < 1 ns and the energy dissipation would be $\sim 10^{-18}$ J.²⁰

IV. CONCLUSIONS

We reported the magnetization switching by the electric field in the ZFO/ZnO heterostructure. The occurrence of magnetization reversal in the heterostructure was attributed to the strain-mediated ME coupling between the polarization of the ZnO film and the magnetization of the ZFO film. A remarkably high value of the ME coupling coefficient for the ZFO/ZnO heterostructure has also been obtained in this investigation. However, it is anticipated that the realization of electric field-induced magnetization switching in the ZFO/ZnO heterostructure will be a very promising aspect of creating energy-efficient spintronic devices.

ACKNOWLEDGMENTS

S.G. acknowledges the Microscience Laboratory, Department of Physics, IIT Kharagpur, for the use of the PLD facility and XRD

system. The author acknowledges the Organic Electronics Laboratory (ORELA), Department of Physics, IIT Kharagpur, for the use of the Thermal Evaporation System to fabricate the Au-electrodes, and the Central Research Facility (CRF), IIT Kharagpur, for the FESEM study. However, S.G. also acknowledges the Department of Science and Technology (DST), India, for giving the INSPIRE Fellowship (Grant No. DST/INSPIRE Fellowship/2016/IF160507) in the course of the work.

AUTHOR DECLARATIONS

Conflict of Interest

The authors have no conflicts to disclose.

Author Contributions

Suman Guchhait: Conceptualization (lead); Data curation (lead); Formal analysis (lead); Investigation (lead); Writing – original draft (lead). **H. Aireddy:** Formal analysis (supporting). **Sudarshan Singh:** Formal analysis (supporting). **Sayan Chakraborty:** Writing – review & editing (supporting). **Niladri Sekhar Kander:** Writing – review & editing (supporting). **A. K. Das:** Conceptualization (lead); Formal analysis (lead); Supervision (lead); Writing – review & editing (lead).

DATA AVAILABILITY

All the data related to this study are available from the corresponding author upon reasonable request.

REFERENCES

- 1 S. A. Wolf, D. D. Awschalom, R. A. Buhrman, J. M. Daughton, V. S. von Molnár, M. L. Roukes, A. Y. Chtchelkanova, and D. M. Treger, *Science* **294**, 1488 (2001).
- 2 S. Ikegawa, F. B. Mancoff, J. Janesky, and S. Aggarwal, *IEEE Trans. Electron Devices* **67**, 1407 (2020).
- 3 S. Bhatti, R. Sbiaa, A. Hirohata, H. Ohno, S. Fukami, and S. N. Piramanayagam, *Mater. Today* **20**, 530 (2017).
- 4 J. Puebla, J. Kim, K. Kondou, and Y. Otani, *Commun. Mater.* **1**, 1 (2020).
- 5 C. Chappert, A. Fert, and F. N. Van Dau, *Nat. Mater.* **6**, 813 (2007).
- 6 J. Åkerman, *Science* **308**, 508 (2005).
- 7 S. Parkin, X. Jiang, C. Kaiser, A. Panchula, K. Roche, and M. Samant, *Proc. IEEE* **91**, 661 (2003).
- 8 S. Tehrani, J. M. Slaughter, E. Chen, M. Durlam, J. Shi, and M. DeHerren, *IEEE Trans. Magn.* **35**, 2814 (1999).
- 9 S. Fukami, T. Anekawa, C. Zhang, and H. Ohno, *Nat. Nanotechnol.* **11**, 621 (2016).
- 10 G. Yu, P. Upadhyaya, Y. Fan, J. G. Alzate, W. Jiang, K. L. Wong, S. Takei, S. A. Bender, L. T. Chang, Y. Jiang, M. Lang, J. Tang, Y. Wang, Y. Tserkovnyak, P. K. Amiri, and K. L. Wang, *Nat. Nanotechnol.* **9**, 548 (2014).
- 11 Y. Fan, P. Upadhyaya, X. Kou, M. Lang, S. Takei, Z. Wang, J. Tang, L. He, L. T. Chang, M. Montazeri, G. Yu, W. Jiang, T. Nie, R. N. Schwartz, Y. Tserkovnyak, and K. L. Wang, *Nat. Mater.* **13**, 699 (2014).
- 12 J. C. Sankey, Y. T. Cui, J. Z. Sun, J. C. Slonczewski, R. A. Buhrman, and D. C. Ralph, *Nat. Phys.* **4**, 67 (2008).
- 13 L. Liu, C. F. Pai, Y. Li, H. W. Tseng, D. C. Ralph, and R. A. Buhrman, *Science* **336**, 555 (2012).
- 14 A. R. Mellnik, J. S. Lee, A. Richardella, J. L. Grab, P. J. Mintun, M. H. Fischer, A. Vaezi, A. Manchon, E. A. Kim, N. Samarth, and D. C. Ralph, *Nature* **511**, 449 (2014).

- ¹⁵H. Aireddy and A. K. Das, *Rev. Sci. Instrum.* **90**, 103905 (2019).
- ¹⁶K. Roy, Hybrid spintronics and straintronics: An ultra-low-energy computing paradigm, Doctoral dissertation, Virginia Commonwealth University, 2012.
- ¹⁷D. C. Ralph and M. D. Stiles, *J. Magn. Magn. Mater.* **320**, 1190 (2008).
- ¹⁸T. H. Lahtinen, K. J. Franke, and S. van Dijken, *Sci. Rep.* **2**(1), 258 (2012).
- ¹⁹S. Fujii, T. Usami, Y. Shiratsuchi, A. M. Kerrigan, A. M. Yatmeidhy, S. Yamada, T. Kanashima, R. Nakatani, V. K. Lazarov, T. Oguchi, Y. Gohda, and K. Hamaya, *NPG Asia Mater.* **14**, 1 (2022).
- ²⁰A. K. Biswas, H. Ahmad, J. Atulasimha, and S. Bandyopadhyay, *Nano Lett.* **17**, 3478 (2017).
- ²¹M. Bibes and A. Barthélémy, *Nat. Mater.* **7**, 425–426 (2008).
- ²²R. Ramesh and N. A. Spaldin, *Nat. Mater.* **6**, 21 (2007).
- ²³J. M. Hu, L. Q. Chen, and C. W. Nan, *Adv. Mater.* **28**, 15 (2016).
- ²⁴M. Liu, T. Nan, J. M. Hu, S. S. Zhao, Z. Zhou, C. Y. Wang, Z. D. Jiang, W. Ren, Z. G. Ye, L. Q. Chen, and N. X. Sun, *NPG Asia Mater.* **8**, 316 (2016).
- ²⁵H. Schmid, *Ferroelectrics* **161**, 1 (1994).
- ²⁶M. Fiebig, *J. Phys. D: Appl. Phys.* **38**, R123 (2005).
- ²⁷W. Eerenstein, N. D. Mathur, and J. F. Scott, *Nature* **442**, 759 (2006).
- ²⁸T. Kimura, T. Goto, H. Shintani, K. Ishizaka, T. H. Arima, and Y. Tokura, *Nature* **426**, 55 (2003).
- ²⁹N. Hur, S. Park, P. A. Sharma, J. S. Ahn, S. Guha, and S. W. Cheong, *Nature* **429**, 392 (2004).
- ³⁰C. W. Nan, M. I. Bichurin, S. Dong, D. Viehland, and G. Srinivasan, *J. Appl. Phys.* **103**, 031101 (2008).
- ³¹G. Srinivasan, *Annu. Rev. Mater. Res.* **40**, 153 (2010).
- ³²W. Jahjah, J. P. Jay, Y. Le Grand, A. Fessant, A. R. Prinsloo, C. J. Sheppard, D. T. Dekadjevi, and D. Spenato, *Phys. Rev. Appl.* **13**(2), 034015 (2020).
- ³³H. Zheng, J. Wang, S. E. Lofland, Z. Ma, L. Mohaddes-Ardabili, T. Zhao, L. Salamanca-Riba, S. R. Shinde, S. B. Ogale, F. Bai, D. Viehland, Y. Jia, D. G. Schlom, M. Wuttig, A. Roytburd, and R. Ramesh, *Science* **303**, 661 (2004).
- ³⁴F. Zavaliche, H. Zheng, L. Mohaddes-Ardabili, S. Y. Yang, Q. Zhan, P. Shafer, E. Reilly, R. Chopdekar, Y. Jia, P. Wright, D. G. Schlom, and R. Ramesh, *Nano Lett.* **5**, 1793 (2005).
- ³⁵F. Zavaliche, T. Zhao, H. Zheng, F. Straub, M. P. Cruz, P. L. Yang, D. Hao, and R. Ramesh, *Nano Lett.* **7**, 1586 (2007).
- ³⁶H. Y. Lyu, Z. Zhang, J. Y. You, Q. B. Yan, and G. Su, *J. Phys. Chem. Lett.* **13**, 11405 (2022).
- ³⁷N. A. Hill, *J. Phys. Chem. B* **104**, 6694 (2000).
- ³⁸J. Lian, F. Ponchel, N. Tiercelin, Y. Chen, D. Rémiens, T. Lasri, G. Wang, P. Pernod, W. Zhang, and X. Dong, *Appl. Phys. Lett.* **112**, 162904 (2018).
- ³⁹J. Wang, Q. K. Huang, S. Y. Lu, Y. F. Tian, Y. X. Chen, L. H. Bai, Y. Dai, and S. S. Yan, *Appl. Phys. Lett.* **112**, 152904 (2018).
- ⁴⁰C. Jiang, C. Zhang, C. Dong, D. Guo, and D. Xue, *Appl. Phys. Lett.* **106**, 122406 (2015).
- ⁴¹S. K. Patel, D. D. Robertson, S. S. Cheema, S. Salahuddin, and S. H. Tolbert, *Nano Lett.* **23**, 3267 (2023).
- ⁴²S. Guchhait, H. Aireddy, N. S. Kander, S. Biswas, and A. K. Das, *J. Appl. Phys.* **131**, 153903 (2022).
- ⁴³R. Adhikari, A. Sarkar, M. V. Limaye, S. K. Kulkarni, and A. K. Das, *J. Appl. Phys.* **111**, 073903 (2012).
- ⁴⁴R. Barman and D. Kaur, *Appl. Phys. Lett.* **108**, 092404 (2016).
- ⁴⁵P. A. Dowben, D. E. Nikonov, A. Marshall, and C. Binek, *Appl. Phys. Lett.* **116**, 080502 (2020).
- ⁴⁶J. Zhai, Z. Xing, S. Dong, J. Li, and D. Viehland, *Appl. Phys. Lett.* **88**, 062510 (2006).